

A calcineurin homologous protein is required for sodium-proton exchange events in the *C. elegans* intestine

Jamie Wagner, Erik Allman, Ashley Taylor, Kiri Ulmschneider, Timothy Kovanda, Bryne Ulmschneider, Keith Nehrke and Maureen A. Peters

Am J Physiol Cell Physiol 301:C1389-C1403, 2011. First published 24 August 2011;
doi:10.1152/ajpcell.00139.2011

You might find this additional info useful...

Supplemental material for this article can be found at:

<http://ajpcell.physiology.org/content/suppl/2011/09/01/ajpcell.00139.2011.DC1.html>

This article cites 70 articles, 37 of which can be accessed free at:

<http://ajpcell.physiology.org/content/301/6/C1389.full.html#ref-list-1>

Updated information and services including high resolution figures, can be found at:

<http://ajpcell.physiology.org/content/301/6/C1389.full.html>

Additional material and information about *AJP - Cell Physiology* can be found at:

<http://www.the-aps.org/publications/ajpcell>

This information is current as of March 8, 2012.

A calcineurin homologous protein is required for sodium-proton exchange events in the *C. elegans* intestine

Jamie Wagner,¹ Erik Allman,² Ashley Taylor,¹ Kiri Ulmschneider,¹ Timothy Kovanda,¹ Bryne Ulmschneider,¹ Keith Nehrke,³ and Maureen A. Peters¹

¹Department of Biology, Oberlin College, Oberlin, Ohio; ²Department of Pharmacology and Physiology, University of Rochester School of Medicine and Dentistry, Rochester, New York; and ³Department of Medicine, University of Rochester School of Medicine and Dentistry, Rochester, New York

Submitted 3 May 2011; accepted in final form 18 August 2011

Wagner J, Allman E, Taylor A, Ulmschneider K, Kovanda T, Ulmschneider B, Nehrke K, Peters MA. A calcineurin homologous protein is required for sodium-proton exchange events in the *C. elegans* intestine. *Am J Physiol Cell Physiol* 301: C1389–C1403, 2011. First published August 24, 2011; doi:10.1152/ajpcell.00139.2011.—*Caenorhabditis elegans* defecation is a rhythmic behavior, composed of three sequential muscle contractions, with a 50-s periodicity. The motor program is driven by oscillatory calcium signaling in the intestine. Proton fluxes, which require sodium-proton exchangers at the apical and basolateral intestinal membranes, parallel the intestinal calcium flux. These proton shifts are critical for defecation-associated muscle contraction, nutrient uptake, and longevity. How sodium-proton exchangers are activated in time with intestinal calcium oscillation is not known. The posterior body defecation contraction mutant (*pbo-1*) encodes a calcium-binding protein with homology to calcineurin homologous proteins, which are putative cofactors for mammalian sodium-proton exchangers. Loss of *pbo-1* function results in a weakened defecation muscle contraction and a caloric restriction phenotype. Both of these phenotypes also arise from dysfunctions in pH regulation due to mutations in intestinal sodium-proton exchangers. Dynamic, in vivo imaging of intestinal proton flux in *pbo-1* mutants using genetically encoded pH biosensors demonstrates that proton movements associated with these sodium-proton exchangers are significantly reduced. The basolateral acidification that signals the first defecation motor contraction is scant in the mutant compared with a normal animal. Luminal and cytoplasmic pH shifts are much reduced in the absence of PBO-1 compared with control animals. We conclude that *pbo-1* is required for normal sodium-proton exchanger activity and may couple calcium and proton signaling events.

caloric restriction; *Caenorhabditis elegans*; motor program; rhythmic behavior; defecation

FINE-TUNED REGULATION OF PROTON distribution and concentration is essential to cell functionality and viability. Protein folding/activity, energy generation, and neurotransmitter loading all depend on appropriate proton concentrations in distinct cellular compartments (10). Proton movement across the cell membrane can also contribute, both directly and indirectly, to various physiological functions, including electrolyte absorption in the kidney and lower gastrointestinal track (10, 19). The importance of proton transport is highlighted by the fact that its timing and magnitude is fine-tuned in response to changes in diet and energy demands by multiple hormonal and growth factor pathways (21, 45). In the kidney's proximal tubules, where the majority of sodium is salvaged from the filtrate,

the activity of a sodium-proton exchanger (NHE3) can be rapidly upregulated by glucocorticoids or decreased by adenosine (6, 18).

The established functions of protons in preserving cellular homeostasis have been expanded in recent years to include intra- and intercellular signaling. Localized sodium-proton exchange can affect cell morphology, polarity, and migration by modifying the actin cytoskeleton (16, 17, 33, 56, 64). Moreover, recent research has demonstrated that extracellular proton fluctuations contribute to the molecular basis of a wide repertoire of cognitive behaviors and physiologic responses in vertebrates via acid-sensing ion channels of the epithelial sodium channel/degenerin family (30, 65–68, 70). If localized proton movements are critical to altering the behaviors of many diverse cell types, the proteins responsible for transporting the protons should be widely expressed.

The sodium-proton exchanger family contains many genes that are broadly expressed, making these transporters well positioned to mediate proton signaling events. Sodium-proton exchangers, called NHEs or NHXs, depending on the organism, are 12-pass transmembrane proteins that typically control the electroneutral exchange of one extracellular sodium ion for one intracellular proton (33, 57). Their long cytoplasmic carboxyl terminal tails contain multiple binding and phosphorylation sites that serve regulatory functions (57). Many organisms possess more than five sodium-proton exchangers (33, 44, 57). Some of these exchangers are expressed ubiquitously, while others are restricted to specific tissues and/or cellular subdomains (10, 33, 57). NHE activity is implicated broadly in the maintenance of cell volume, electrolyte transport, and cytoplasmic pH levels (10, 33, 57). More specialized functions of sodium-proton exchangers have been noted in particular cell lines, including contributions to cell migration, morphology, proliferation, apoptosis, and tumor metastasis (11, 15, 16, 24, 27, 36, 49, 52–54, 63). The striking multiplicity of reported NHE functions suggests that these proteins may act in a highly context-dependent manner.

In *Caenorhabditis elegans*, recent work has provided evidence that sodium-proton exchangers can mediate acute cell signaling (7, 51). Proton signaling instructs part of *C. elegans* defecation, a rhythmic behavior composed of three sequential muscle contractions [Fig. 1A; (12, 61)]. Oscillatory calcium signaling in the intestine controls the periodicity and initial signals for the motor program (14). The first contraction, the posterior body contraction, is triggered by the calcium-mediated secretion of a signaling molecule directly from the intestinal cells (50). These intestinally derived signaling molecules are protons. Proton extrusion via a basolateral intestinal sodium-proton exchanger, PBO-4/NHX-7, is

Address for reprint requests and other correspondence: M. Peters, Dept. of Biology, Oberlin College, Oberlin, OH 44074 (e-mail: maureen.peters@oberlin.edu).

both necessary and sufficient to induce the posterior body contraction (7, 51). This finding demonstrates a novel function for sodium-proton exchangers in fast cell-cell communication through the secretion of protons.

A separate sodium-proton exchanger that resides at the apical intestinal membrane, NHX-2, contributes to defecation along with several other physiologic processes (41, 51). Protons move from the acidic intestinal lumen into the cytoplasm and are subsequently pumped back into the lumen by the vacuolar H⁺-ATPase (1, 51). A reduction in NHX-2 function dampens proton movement across the apical membrane and affects posterior body contraction and the frequency of defecation (51). Reduced nutrient uptake and a lengthened lifespan are also evident in this mutant, presumably due to the physiological coupling of NHX-2 activity to that of the peptide-proton symporter OPT-2/PEPT-1 (41). These observations highlight the unique ability of a single transporter to influence multiple integrated processes.

Activation of both NHX-2 and PBO-4/NHX-7 is precisely timed to match the defecation cycle's initiation, suggesting that their activities are regulated by the defecation "clock." A critical component of the defecation cycle timing is 1,4,5 inositol trisphosphate receptor calcium release that initiates a calcium wave (14, 20, 43, 50, 59). Therefore proton release, like the release of many traditional neurotransmitters, must be signaled directly or indirectly by transient calcium spike. The pathway linking calcium ions to activation of sodium-proton exchange is largely unknown.

In this study, we have identified a new and severe posterior body contraction mutant, *pbo-1*. Mutation of this calcium-binding protein, with homology to calcineurin homologous proteins (*chps*), causes profound deficits in posterior body contraction that exceed those of the *pbo-4/nhx-7* mutants. Vertebrate CHPs bind and can regulate sodium-proton exchangers (17, 18, 22, 28, 48, 69). We hypothesize that PBO-1 is required for sodium-proton exchanger activity. *C. elegans pbo-1* loss-of-function mutants display drastic decreases in the intestinal proton movements associated with PBO-4/NHX-7 and NHX-2 function. Proton movements across the basolateral and apical intestinal membranes are reduced, as is the strength of the associated muscle contraction. Furthermore, nutrient uptake appears to be compromised. The *pbo-1* mutants display an extremely low level of intestinal fat stores, consistent with diminished NHX-2 activity. These data demonstrate that PBO-1/CHP regulates at least two intestinal sodium-proton exchangers in *C. elegans*. Our work demonstrates that worms provide a unique and novel organism in which to study the global effects of losing CHP function.

MATERIALS AND METHODS

Strains

Nematodes were cultured using standard methods (9). The wild type is the N2 isolate from Bristol, England. *pbo-1* mutant strains are TA105 *pbo-1(sa7)*III and TA111 *pbo-1(tm3716)*III. *sa7* was originally identified by J. Thomas in an EMS screen (61). It was then outcrossed seven times in the Peters Lab to generate TA105 (61). *tm3716* was isolated by the National BioResource Project for the Experimental Animal *C. elegans* and is described on Wormbase (<http://www.wormbase.org>). TA111 was derived by outcrossing FX3716 *pbo-1(tm3716)* four times. *pbo-1* expression analysis was done using strain KWN21 *unc-119(e2498)*III; *rnyEx005* [*Ppbo-1::GFP*; pPDM016B (*unc-119+*)]. The following strains were used for behavioral assays: TA105 *pbo-1(sa7)* III, TA111 *pbo-1(tm3716)* III,

RB793 *pbo-4/nhx-7(ok583)*X, TA124 *pbo-1(tm3716)* III, *obEx10* [*Pvit-2::PBO-1*; *Punc-122::GFP*]. For fluorescent calcium imaging, strains KWN2 *pha-1(e2123ts)*III; *unc-31(n422)*IV; *rnyEx001* [*Pnhx-2::YC6.1*; *pha-1(+)*], TA107 *pbo-1(sa7)*III; *unc-31(n422)*IV; *rnyEx001* [*Pnhx-2::YC6.1*; *pha-1(+)*], and TA113 *pbo-1(tm3716)*III; *rnyEx001* [*Pnhx-2::YC6.1*; *pha-1(+)*] were used. Calcium flux was analyzed in *nhx-2(RNAi)* mutants by feeding KWN2 *pha-1(e2123ts)*III; *unc-31(n422)*IV; *rnyEx001* [*Pnhx-2::YC6.1*; *pha-1(+)*] animals bacteria expressing the plasmid pRNAi-*nhx-2* for two generations (41). Pseudocoelomic pH was studied using strains KWN30 *pha-1(e2123ts)*III; *rnyEx009* [*Ppbo-4/nhx-7::PAT-3::pHluorin*, *pha-1(+)*] and KWN31 *pbo-4/nhx-7(ok583)*X; *pha-1(e2123ts)*III; *rnyEx009* [*Ppbo-4/nhx-7::PAT-3::pHluorin*, *pha-1(+)*]. The *rnyEx009* array was crossed into *pbo-1(sa7)* and (*tm3716*)III for imaging purposes; stable lines were not isolated. For cytoplasmic intestinal pH imaging, strains KWN26 *pha-1(e2123ts)*III; *him-5(e1490)*V; *rnyEx006* [*Pnhx-2::pHluorin*], TA106 *pbo-1(sa7)*III; *him-5(e1490)*V; *rnyEx006* [*Pnhx-2::pHluorin*; *pha-1(+)*] and TA114 *pbo-1(tm3716)*III; *him-5(e1490)*V; *rnyEx006* [*Pnhx-2::pHluorin*; *pha-1(+)*] were used. Cytoplasmic pH flux was analyzed in *nhx-2(RNAi)* mutants by feeding KWN26 *pha-1(e2123ts)*III; *him-5(e1490)*V; *rnyEx006* [*Pnhx-2::pHluorin*; *pha-1(+)*] animals bacteria expressing the plasmid pRNAi-*nhx-2* for two generations (41).

Genetic Analysis and Behavioral Assays

A normal defecation cycle consists of a posterior body contraction, followed by an anterior body contraction and finally an enteric muscle contraction (61). In individuals lacking visible posterior body contractions, e.g., all *pbo-1(tm3716)*, all *sa7/tm3716*, and 3 of 11 *sa7*, cycles were defined by the presence of enteric muscle contractions. Actively feeding first- or second-day adults were visually assayed at room temperature (20–22°C) for 10 motor programs on a nematode growth medium (NGM) plate with the lid on. Eleven animals were scored for all genotypes. Because of the difficulty of scoring the anterior body contractions of the *pbo-1* mutants, these contractions were scored in separate assays that focused primarily on the anterior segment. Statistical significance was calculated using two-tailed unpaired Student's *t*-tests with unequal variance.

Rescuing Construct

The rescuing array, pMAP10, was created as follows. The *vitellogenin-2* (*vit-2*) minimal promoter fragment was amplified using primers that added a 5'-*Pst* I site (5'-tgctgcagattactgaacaatttag-3') and a 3'-*Bam*H I site (5'-caggatccggggctgaaccgtg-3') and cloned into the Blunt PCR cloning vector, pSC-B (Stratagene) (31). The minimal *Pvit-2* fragment was removed from pSC-B by *Pst* I/*Bam*H I digestion and cloned into a *Pst* I/*Bam*H I cut pMAP9 vector. The pMAP9 vector is a derivative of pPD95.75 containing *pbo-1* cDNA without a green fluorescent protein (GFP) tag. pMAP9 contains the following: ~2 kb *pbo-1* 5'-regulatory sequence promoter cloned between *Pst* I and *Bam*H I (amplified using 5-actctgcagtgtcccattttgcccagg-3' and 5'-ggatccgatattgtgttttgaagaattagatgtg-3'), a *pbo-1* cDNA with an artificial intron (5'-gtaagttaaacatataactaactaacccatggattttaaatttcag-3') inserted into the *Eco*RV site of the *pbo-1* cDNA, followed directly by the *unc-54* 3'-untranslated region (UTR) (8). The *pbo-1* cDNA was originally amplified by RT-PCR on whole worm RNA and the open reading frame was sequenced in both directions. Transgenic array strains were generated by standard microinjection techniques. Rescuing arrays were obtained by injecting 10 ng/ml pMAP10, 13.4 ng/ml *Punc-122::GFP* [coelomocyte:GFP] (39), and 76.6 ng/ml DNA ladder to generate the extrachromosomal array *obEx10*. Several rescuing transgenic arrays, *obEx10–12*, were created and produced visible recovery of mutant phenotypes.

GFP Construct

A GFP transcriptional reporter was a PCR fragment composed of ~2 kb of the *pbo-1* promoter fragment and GFP with an *unc-54*

3'-UTR and was generated by a two-step PCR procedure. During the initial PCR amplification, the *pbo-1* promoter was modified to delete the start codon and incorporate the 3'-GFP sequence using the following primers: 5'-CCCATTTTGGCGCAGGATTGTGCTG-3' and 5'-ACATACCTTTGGGTCCTTTGGGAATTTGGCCCAATCTGTAGATTGG-3'. A separate PCR amplified a fragment containing GFP and the *unc-54* 3'-UTR. These two PCR fragments were then annealed and amplified using the outside primers from the initial PCRs. The *Ppbo-1::GFP* fragment was isolated and purified. A transcriptional reporter array, *myEx005*, was generated by injecting 10 ng/ml of the *Ppbo-1::GFP* PCR fragment, 75 ng/ml of pPDM016B [*unc-119+*], and 65 ng/ml of 1 kb DNA ladder into *unc-119(e2498)III* mutants to generate strain KWN21.

Standard Microscopy

Fluorescence images of worms expressing *Ppbo-1::GFP* were obtained using a Zeiss LSM5 Pascal confocal microscope with a total magnification of $\times 400$. Minor adjustments were made to the green level (from 40% to 80%) when transitioning from color to grayscale to maintain image fidelity and highlight the location of the observed fluorescent signal.

To determine relative contraction strength, defecation cycles of wild-type, *pbo-1*, and *pbo-4* (strains: TA105, TA111, and RB793) animals on worm plates were digitally recorded using a Leica MZF-LIII dissecting microscope equipped with a digital Olympus DP72 camera. Using the Leica recording program, DP2-BSW, the distance between the animal's posterior intestine and vulva was manually marked and then digitally measured under two conditions: 1) immediately preceding posterior body contraction and 2) during maximal posterior body contraction. The difference in length was determined as follows: 1-(max contraction length/precontraction length), 3 cycles per worm. Contraction strength was normalized to the average for wild-type worms and is expressed as a percentage.

Fluorescent Indicator Microscopy and Analysis

Relative proton and calcium fluxes were measured in live, feeding, and moving worms (42, 43, 51). Larval stage 2 (L2), L3, and young adult worms were placed on a NGM agarose plate seeded with dilute OP50 *Escherichia coli*. Images were acquired as previously described (42, 51). In brief, a Nikon TE2000U inverted microscope coupled to a Cooke Senscam CCD camera, Polychrome IV monochromatic light (TILL Photonics), and, for *cameleon* only, an Optical Insights beamsplitter were used (42, 51). Data collection and analyses were conducted using the TILLvisION software program and Microsoft Excel. Signal was optimized using background subtraction of signal from plate region without worms and thresholding. Three hundred-second movies were taken of each individual. Manual manipulation of the microscope stage kept freely moving worms within view. Rapid stage movement occasionally induced a short segment of noise, a short large spike in the *y*-axis, as seen in Figs. 5E and 6E.

Cameleon. Strains KWN2, TA107, and TA113 were used. A cyan fluorescent protein/yellow fluorescent protein filter, 435 nm excitation (50 ms), dual emissions, 480 and 535 nm, and 2×2 binning was used. Change in pixel-by-pixel signal was determined as R/R_0 : emission ratio (*R*) divided by initial emission ratio (R_0).

pH measurements. Strains KWN26, TA106, TA114, and *nhx-2RNAi*-treated KWN26 were used for cytoplasmic pHluorin measurements. Animals containing the *myEx009* [*Pnhx-7::PAT-3::pHluorin, pha-1(+)*] array stably, KWN30 and KWN31, or transiently, TA105 and TA111 were used for imaging pseudocolemic pHluorin. pHluorin measurements were obtained with the following settings: sequential 410/470 nm excitation (10 ms), a 500 dichroic filter, and 535 emissions (2×2 binning). For luminal pH measurements, an indicator (1 mg/ml Oregon Green 488 Dextran, Molecular Probes) was loaded into the following strains: N2, TA105, TA111, and *nhx-2RNAi*-treated KWN26 as previously described (42, 51). The

settings and procedure of Oregon Green image acquisition were similar to that for pHluorin worms, with the exceptions of a 440/490 excitation (20 ms) and 515 dichroic filter. Fluorescence was converted to approximate pH units using a signal calibration formula, determined using an in situ high potassium-nigericin technique (60).

Analyses. The resting pH levels and the amplitude of calcium or pH change during a cycle were determined for each worm's trace. Amplitude was based on the difference between resting level and the highest or lowest point. All values, i.e., maximum, minimum, or resting level, were averages of a set of four points. For each indicator and genotype, the period, resting pH, and change amplitudes were averaged to find the mean \pm SE.

Oil Red-O Stain

Oil Red-O (5.0 mg/ml) was used to stain body fat stores as previously described (58). N2, TA105, TA111, and *nhx-2 (RNAi)* treated worms were assayed and photographed. A pool of ~ 100 worms were stained and viewed. Several representative animals of each genotype were photographed.

RESULTS

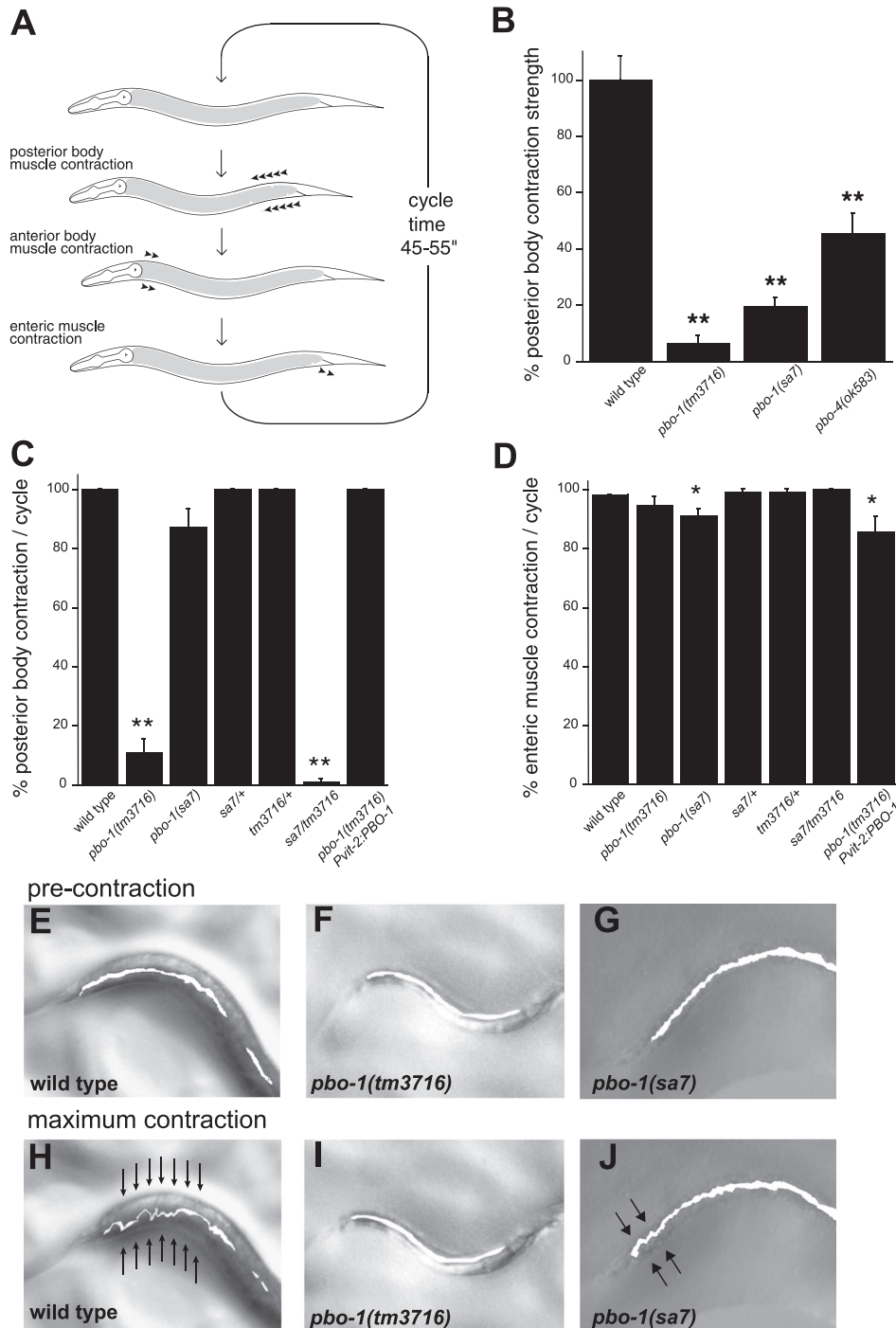
pbo-1 mutants lack normal posterior body contractions. The first muscle contraction of the *C. elegans* defecation motor program, the posterior body contraction, is controlled by direct signaling between the intestine and the body wall muscles (14, 20, 43, 59). Calcium signaling in the intestine times the motor program and instructs the motor output (14, 20, 43, 46). Two posterior body contraction (*pbo*) mutants, *pbo-4* and *pbo-5*, that specifically diminish this contraction have been characterized (7, 51, 61). *pbo-4*, a sodium-proton exchanger, and *pbo-5*, a proton-gated ion channel, comprise a rapid proton signaling pathway that culminates in muscle contraction (7, 51). To further elucidate the molecular components that contribute to this novel signaling pathway, another gene whose mutation causes profound defects in posterior body contraction, termed *pbo-1*, was analyzed (Fig. 1, B–J).

Two *pbo-1* alleles exist. The *pbo-1(sa7)* allele is recessive and was isolated in an EMS screen for defecation mutants (61). *pbo-1(sa7)* mutants display slow development, reduced body size, and fecundity [growth (time to adulthood): *pbo-1(sa7)*, 5 days; N2, 3 days, and brood size: *pbo-1(sa7)*, 74 ± 10 , N2, 246 ± 14]. Standard genetic mapping and complementation techniques were used to identify the gene mutated in the *pbo-1(sa7)* as Y71H2AL.1 (see below). A deletion allele, *pbo-1(tm3716)*, was subsequently generated by the Japanese National BioResource Project. Although the *tm3716* allele was originally reported to be lethal, the *tm3716* animals are fully viable, though small and sickly like the *sa7* allele. Both alleles display severely reduced posterior body contraction strength in comparison to wild type [Fig. 1B; Supplemental Movies 1 and 2; N2, $100.0 \pm 9.1\%$; *pbo-1(tm3716)*, $6.5 \pm 2.5\%$, $P < 0.001$; *pbo-1(sa7)* $19.6 \pm 3.0\%$, $P < 0.001$]. The deletion allele results in an almost complete loss of posterior body contraction, whereas *sa7* retains some extremely weak contractions that are detectable in replayed video recordings and/or by a skilled observer (Fig. 1, F, G, I, and J; Supplemental Movies 2 and 3). In a *sa7tm3716* heterozygote, the *tm3716* phenotype, lacking nearly all posterior contraction, is observed. This finding suggests that *tm3716* is a complete loss-of-function allele, whereas *sa7* is a strong loss-of-function allele (Fig. 1, C and D). Surprisingly, the *pbo-1* mutants' contraction strengths are significantly reduced in comparison to the previously isolated

sodium-proton exchanger mutant, *pbo-4/nhx-7* [*pbo-4(ok583)*, $45.5 \pm 6.9\%$, $P < 0.001$, Fig. 1B]. Like some *pbo-4* alleles, *pbo-1* mutation can also cause a reduction in the frequency of enteric muscle contraction [Fig. 1D; N2, $98.2 \pm 1.2\%$; *pbo-1(tm3716)*, $94.6 \pm 2.9\%$; *pbo-1(sa7)*, $90.9 \pm 2.5\%$, $P < 0.05$; (7)]. The *tm3716*, but not the *sa7* allele, exhibits a slight but significant reduction in the frequency of anterior body contractions [N2, $100.0 \pm 0.0\%$; *pbo-1(tm3716)* $93.6 \pm 8.1\%$ $P < 0.05$; *pbo-1(sa7)* $96.4 \pm 6.7\%$]. The composite *pbo-1* phenotypes suggest that the gene mutated in this mutant is a critical component of the proton-mediated posterior contraction signaling pathway.

pbo-1 encodes a Calcineurin Homologous Protein

Using single nucleotide mapping, the *pbo-1(sa7)* mutation was found to occur in a small interval of chromosome III where two predicted genes, Y71H2AL.1 and Y71H2AL.2, reside. RNA interference of Y71H2AL.1 but not Y71H2AL.2 phenocopied the defecation defects of *pbo-1* (A. Taylor and M. A. Peters, unpublished observations). Additional confirmation came from the *tm3716* allele, which, as mentioned above, shares the posterior body contraction and other phenotypes. Y71H2AL.1 has a high percentage of homology to calcineurin



homologous protein CHP and is the third closest *C. elegans* CHP homolog (47% identity, 64% similarity to human CHP1) (5, 28). The two closest CHP homologs have not been fully analyzed because genetic mutants do not exist. Unlike their namesakes, calcineurin homologous proteins do not possess phosphatase activity. Instead, the protein's name reflects the similarity of its EF-hand calcium-binding motifs to those of the calcineurin B regulatory subunit (28). Each *pbo-1* allele contains a mutation within the Y71H2AL.1 open reading frame. Y71H2AL.1, heretofore called *pbo-1*, has two putative EF-hand motifs at its COOH terminus that correspond to the 3rd and 4th EF hands of the vertebrate CHPs (2, 5, 28, 38, 48). The *sa7* allele is a nonconservative substitution, E135K, that reverses the charge of a highly conserved negatively charged residue, the “-Z” position of the calcium-binding loop, in the first *C. elegans* EF hand (13). The *tm3617* allele affects the final two exons of the transcript and deletes the last EF hand completely (69). Finally, *pbo-1* cDNA expression rescues the posterior body contraction deficits of *pbo-1* mutants (Fig. 1, C and D).

Vertebrate calcineurin homologous proteins are multifunctional proteins that act in a variety of cellular compartments and in concert with a number of proteins with disparate functional roles. (33, 35, 48, 69). Biochemical and tissue culture studies suggest that the three vertebrate CHPs have multiple binding partners and cellular functions including membrane trafficking, cytoskeletal organization, rRNA transcription, and regulation of sodium-proton exchange (3–5, 23, 28, 48, 62). Since posterior body contraction is signaled by sodium-proton exchange, PBO-1 may coordinate sodium-proton exchange within the intestine, perhaps in response to periodic calcium signaling. To evaluate the site/s of *pbo-1* action, expression analysis was performed.

PBO-1 Functions in the Intestine

To determine where *pbo-1* is expressed, a transcriptional reporter was generated by cloning ~2 kb of *pbo-1*'s 5' upstream sequence to a promoterless GFP. In transgenic animals expressing this transcriptional promoter fusion, GFP was localized to the intestine and neurons in embryonic, larval, and adult animals (Fig. 2). The earliest observed GFP signal was present in threefold or pretzel-stage embryos (M. A. Peters, unpublished observations). Intestinal expression is fairly even

throughout the length of the intestine of early animals (embryonic and larval stage 1 animals) but becomes weaker in the mid-intestine from larval stage 2 onward (Fig. 2, A and B). Neuronal expression is robust throughout life, with many neurons in the head region apparent (Fig. 2, B–E).

Since mammalian CHP is required for robust sodium-proton exchange activity, and sodium-proton exchange is responsible for the posterior body contraction, the site of CHP's action in this process was expected to be intestinal rather than neuronal (47, 48). To test this prediction, an adult, intestine-specific rescue construct was used to complement the *pbo-1* mutant. Because vertebrate CHP proteins play a significant role in cell morphology and membrane trafficking, it seemed prudent to test whether or not early *pbo-1* expression was required for intestinal differentiation. An egg-specific promoter, *vitellogenin-1*, can reliably direct adult-specific transcription in *C. elegans* (31). Therefore, the minimal *vitellogenin-1* promoter element was used to drive *pbo-1* transcription in the adult intestinal rescue experiment.

Adult intestinal expression of *pbo-1* rescues the posterior body contraction phenotypes (Fig. 1C). Therefore a developmental requirement can be dismissed. This finding is also consistent with the timing of *pbo-1* expression which begins past the genes required for intestinal specification and differentiation (32). These findings clearly demonstrate that PBO-1 directly influences posterior body contraction strength in the mature intestine.

PBO-1 Does Not Alter Calcium Spike Initiation

The localization and structure of PBO-1 suggests that it may coordinate the cyclic intestinal calcium flux with activation of sodium-proton exchange at the intestinal membrane. In this model, PBO-1 would act downstream of the calcium release event, and rhythmic oscillations in intestinal calcium should occur normally in the *pbo-1* mutant. To determine the timing and amplitude of calcium flux during defecation cycles, in vivo calcium imaging was performed. Animals expressing the ratiometric calcium indicator cameleon YC6.1 were imaged without the use of physical immobilization or paralytic agents for several cycles of the motor program (43, 50, 59). In control animals, a spike in calcium occurs at the start of each defecation cycle, approximately every 45–55 s. Calcium levels rise rapidly and then return to resting levels at a slower rate (Fig. 3A; Supplemental Movie 4).

Fig. 1. Characterization of posterior body contraction mutant 1 (*pbo-1*) motor program defects. *A*: defecation cycle in *Caenorhabditis elegans* (50). Worms execute the motor program approximately every 45–55 s while feeding. During the posterior body muscle contraction, the body muscles surrounding the intestine contract as a wave directed toward the anterior, forcing the contents of the gut forward. Approximately 3–5 s later, the anterior body muscles contract, propelling the gut contents backward (anterior body contraction). This is followed about a half-second later by an enteric muscle contraction that opens the anus and forcibly expels waste products. *B*: posterior body contraction strength. Contraction strength percentages normalized to wild-type samples (100%) are shown. Three cycles per animal were scored; $n = 7$ animals for each genotype except *pbo-1(tm3716)*, where $n = 5$ [means \pm SE: wild type $100.0 \pm 9.1\%$; *pbo-1(tm3716)* $6.5 \pm 2.5\%$, $P < 0.001$; *pbo-1(sa7)* $19.6 \pm 3.0\%$, $P < 0.001$; *pbo-4(ok583)* $45.5 \pm 6.9\%$, $P < 0.001$]. $**P < 0.001$ using an unpaired Student's *t*-test with unequal variance. *C*: mean percentage of posterior body contractions per cycle. Ten motor programs were scored per worm, 11 animals per genotype [means \pm SE: wild type, $100.0 \pm 0.0\%$; *pbo-1(tm3716)*, $10.9 \pm 4.6\%$, $P < 0.0001$; *pbo-1(sa7)*, $87.3 \pm 6.0\%$; *pbo-1(sa7)/+*, $100.0 \pm 0.0\%$; *pbo-1(tm3716)/+*, $100.0 \pm 0.0\%$; *pbo-1(sa7)/pbo-1(tm3716)*, $0.9 \pm 0.9\%$, $P < 0.0001$; *pbo-1(tm3716)[Pvit-2:PBO-1]*, $100.0 \pm 0.0\%$]. $**P < 0.0001$ using an unpaired Student's *t*-test with unequal variance. *D*: mean percentage of enteric muscle contractions per cycle. Ten motor programs were scored per worm, 11 animals per genotype [means \pm SD, wild type, $98.2 \pm 1.2\%$; *pbo-1(tm3716)*, $94.6 \pm 2.9\%$; *pbo-1(sa7)*, $90.9 \pm 2.5\%$, $P < 0.05$; *pbo-1(sa7)/+*, $99.1 \pm 1.0\%$; *pbo-1(tm3716)/+*, $99.1 \pm 1.0\%$; *pbo-1(sa7)/pbo-1(tm3716)*, $100.0 \pm 0.0\%$; *pbo-1(tm3716)[Pvit-2:PBO-1]*, $85.5 \pm 5.3\%$, $P < 0.05$]. $*P < 0.05$ using an unpaired Student's *t*-test with unequal variance. *E–J*: representative images of worms during a defecation motor program. Frames were taken from bright field movies. The first row of images shows the animal just before posterior body contraction. The second row displays the animal at maximal posterior body contraction. The lumen of the intestine has been shaded white. *E*: wild-type animal, just prior to contraction. *F*: *pbo-1(tm3716)*, estimated precontraction. Since posterior body contractions are not readily visible in this mutant, the timing of the posterior body contraction was estimated relative to the onset of enteric muscle contraction. *G*: *pbo-1(sa7)*, just before contraction. *H*: wild-type animal at maximal posterior body contraction. Arrows point to region of contraction. *I*: *pbo-1(tm3716)* at estimated maximal posterior body contraction. Since posterior body contractions are not readily visible in this mutant, the timing of the posterior body contraction was estimated relative to the enteric muscle contraction. *J*: *pbo-1(sa7)* at maximal posterior body contraction. Arrows point to small region of contraction.

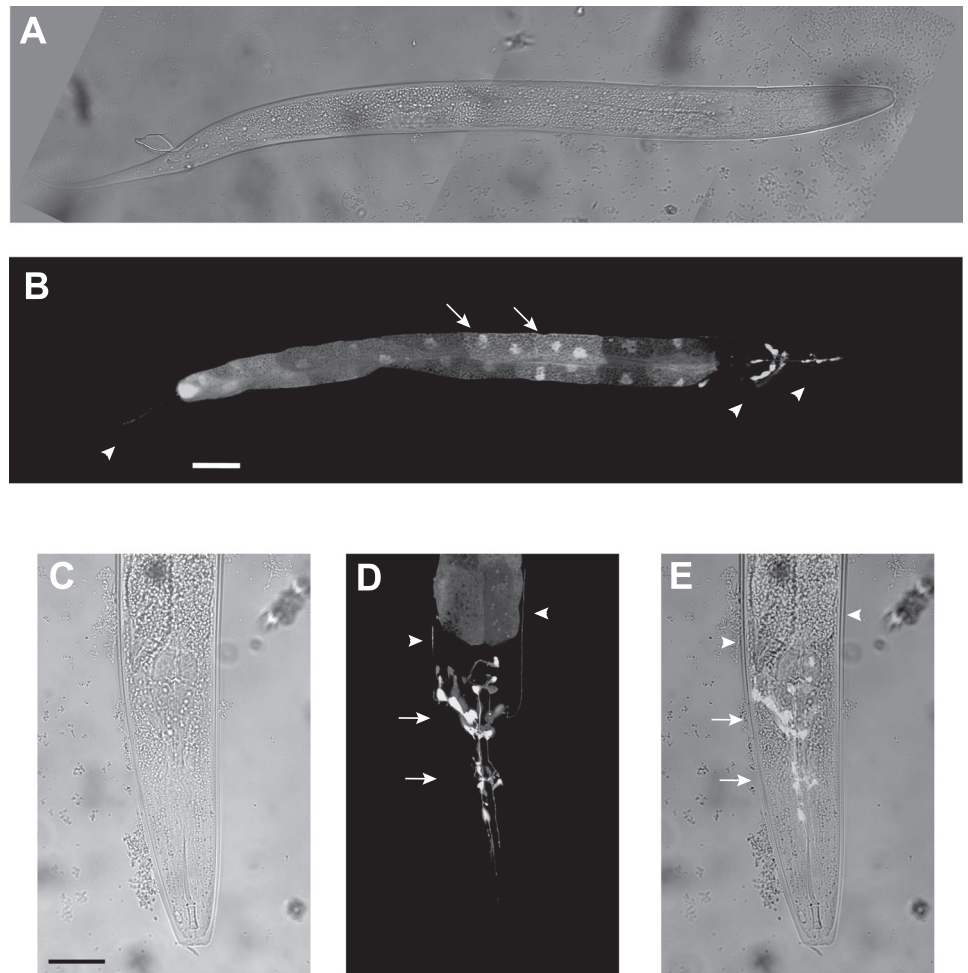


Fig. 2. Expression pattern of *pbo-1*. *A–E*: expression of green fluorescent protein (GFP) driven by the promoter of *pbo-1*, *Ppbo-1::GFP*. *A*: DIC image of an L2 stage animal. Scale bar equals 50 μ m. Anterior is to the right. *B*: fluorescent image of the worm shown in *A*. Fluorescence is observed in the intestine of the larval animal, where it accumulates in the nuclei (seen as bright circles, arrows). Fluorescence is also visible in a number of neurons in the head and one neuronal process in the tail (indicated by arrowheads). *C*: DIC image of the head and anterior intestine of an adult animal. Scale bar equals 50 μ m. *D*: fluorescence image of the animals shown in *C*. Expression is evident in the anterior intestine and many neurons. Fluorescence is found in neuronal processes, likely the anterior pharyngeal nerve ring and terminal bulb (arrows), as well as in the ventral cord (arrowheads). *E*: merged image of *C* and *D*. Arrows and arrowheads mark the same areas as in *D*.

The magnitude of calcium elevation was very similar in *pbo-1* mutant and control animals (Fig. 3, *B*, *C*, *E*, and *F*; Supplemental Movie 5), although it was noted that the rate of return to resting calcium levels appeared to be somewhat delayed in the *sa7* allele, and to a lesser extent in the *tm3617* allele (Fig. 3, *A–C*). This difference between the two *pbo-1* alleles may be caused by residual protein in *sa7*, the weaker loss of function mutant. Since *nhx-2* mutation has been reported to slow the rate of recovery following defecation-associated calcium spike, animals treated with *nhx-2* RNAi were added to the analysis (51). *nhx-2(RNAi)* animals exhibited slow recovery from the calcium spikes but no other significant alteration, matching previous reports (Fig. 3*D*). The frequency of calcium flux and motor programs was not altered consistently in the mutants or in the mutants with fluorescent reporter genes. Observing normal calcium release events in the *pbo-1* mutants suggests that PBO-1 does not affect the central timekeeping mechanism. Rather, PBO-1 is required for events elicited in response to the calcium release.

PBO-1 Is Required for Proton Transmission

The sodium-proton exchanger, PBO-4/NHX-7, is required for proton extrusion from the intestine into the pseudocoelom, the small space between the intestine and the overlying body wall muscles (7, 51). Since this acute acidification of the pseudocoelomic space is required for posterior body contraction, we hypothesized that the *pbo-1* mutants would lack this acidification. To

visualize the pH dynamics of the *pbo-1*'s pseudocoelom, a pH-sensitive indicator, pHluorin, was targeted to the exterior surface of the intestine's basolateral membrane (37, 51, 55).

Pseudocoelomic acidification was much reduced in the *pbo-1* mutants (Fig. 4; Supplemental Movies 6–8). In control animals, a rapid pH drop of ~ 0.5 pH units is associated with initiation of the posterior body contraction [Fig. 4*A*; (7, 51)]. Within approximately 10 s, pseudocoelomic pH returns to resting levels [Fig. 4*A*; (7, 51)]. In the *pbo-1* animals, periodic drops in pH could be discerned, but they were of much lower magnitude (Fig. 4, *B* and *C*; Supplemental Movies 7 and 8). The average amplitude of the *pbo-1* pseudocoelomic acidification was substantially diminished [Fig. 4*F*; control, 0.54 ± 0.07 units; *pbo-1(tm3716)*, 0.15 ± 0.05 , $P < 0.01$; *pbo-1(sa7)*, 0.11 ± 0.01 , $P < 0.01$]. The rate of pH shift, particularly neutralization, tended to be less rapid in the *pbo-1* mutants compared with control; comparison of the slope of control and *pbo-1* mean pH cycles demonstrates this (Fig. 4, *A–C* and *E*). These factors made the selection of many *pbo-1* acidification events difficult. Since PBO-4/NHX-7 is responsible for the bulk of the sodium-proton exchange at this membrane, *pbo-4/nhx-7*-null animals, allele *ok583*, were also assayed for comparative purposes. The observed *pbo-4/nhx-7* results corroborate earlier studies (7, 51). *pbo-4/nhx-7* animals exhibit weaker acidification events and reduced rates of pH change in comparison to control [Fig. 4, *A* and *D*; *pbo-4/nhx-7(ok583)*, $0.14 \pm$

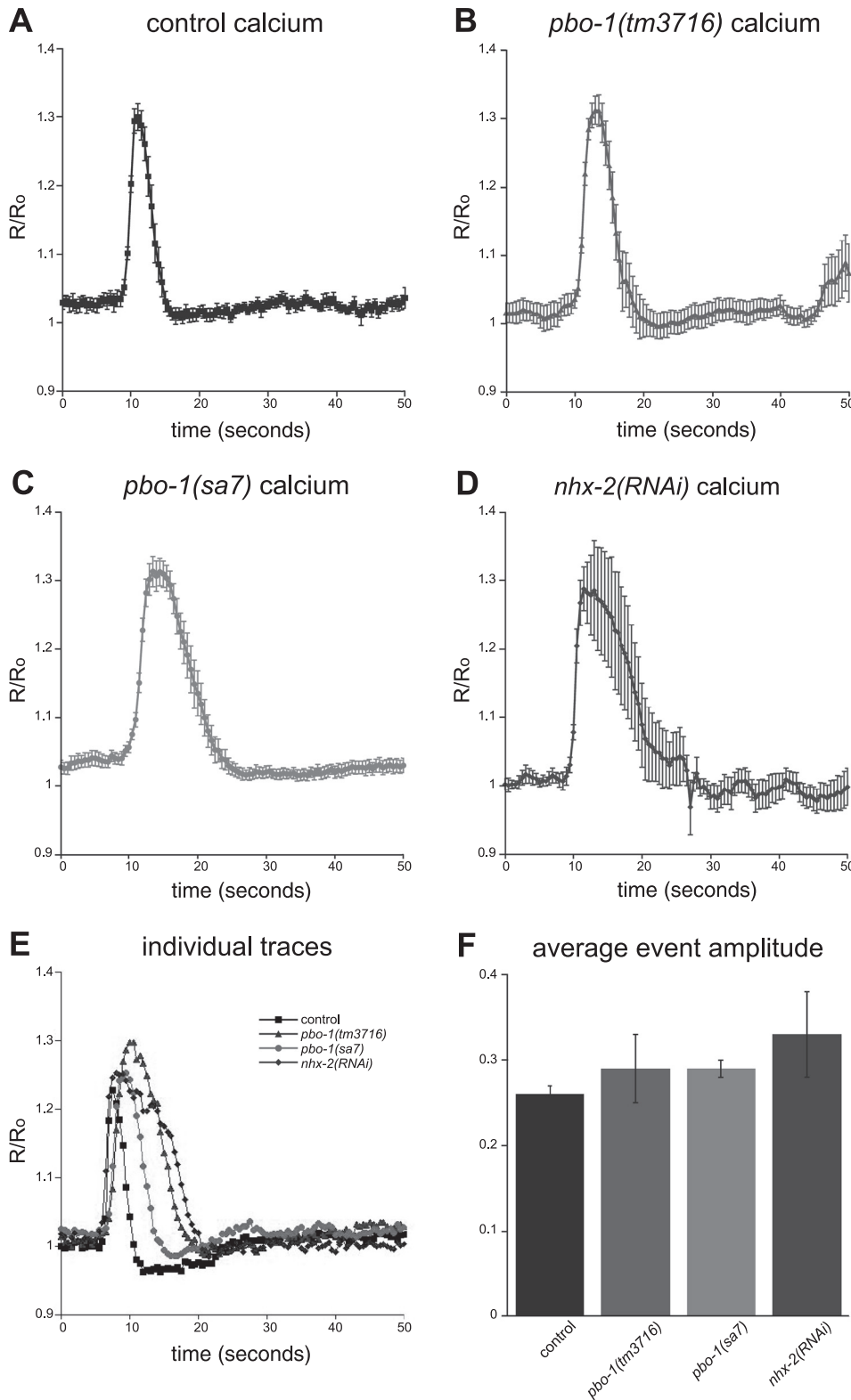


Fig. 3. Intestinal calcium dynamics in control, *pbo-1*, and *nhx-2(RNAi)* animals. A–D: mean change in fluorescence intensity of the calcium indicator, cameleon, for each genotype assayed. The means were determined from one representative cycle per worm. The error bars indicate SE. The y-axis is the ratio (*R*) of fluorescence emission relative to background emission (*R*₀). The x-axis represents time (in s). A: mean calcium change during approximately one defecation cycle period of the control, genotype = *pha-1(e2123ts)III; unc-31(n422)IV; rmyEx001[Pnhx-2::YC61; pha-1(+)]*, *n* = 9. B: mean calcium change during approximately one defecation cycle period of *pbo-1(tm3716)*, genotype = *pbo-1(tm3716)III; rmyEx001[Pnhx-2::YC61; pha-1(+)]*, *n* = 9. C: mean calcium change during approximately one defecation cycle period of *pbo-1(sa7)*, genotype = *pbo-1(sa7)III; unc-31(n422)IV; rmyEx001[Pnhx-2::YC61; pha-1(+)]*, *n* = 10. D: mean calcium change during approximately one defecation cycle period of *nhx-2(RNAi)*, genotype = *pha-1(e2123ts)III; unc-31(n422)IV; rmyEx001[Pnhx-2::YC61; pha-1(+)]*, feed pRNAi-*nhx-2*, *n* = 6. E: graph with one sample trace for each genotype shown in A–D. ■, control genotype (A); ▲, *pbo-1(tm3716)* (B); ●, *pbo-1(sa7)* (C); ◆, *nhx-2(RNAi)* (D). F: mean amplitude of calcium change for genotypes in A–D. This mean incorporates every defecation cycle successfully recorded for each genotype. The total number of individual animals scored is listed above. Means ± SE are as follows: control, 0.26 ± 0.01; *pbo-1(tm3716)*, 0.29 ± 0.01; *pbo-1(sa7)*, 0.29 ± 0.04; *nhx-2(RNAi)*, 0.33 ± 0.05.

0.02, *P* < 0.01]. The average amplitudes of the remaining *pbo-4/nhx-7* and *pbo-1* pH flux events are very similar (Fig. 4, E and F). Mutation of both *pbo-1* and *pbo-4/nhx-7* analogously alter the proton signal that initiates posterior body contraction, suggesting that PBO-1 may act to regulate PBO-4/NHX-7 activity.

PBO-1 As a Global Regulator of Sodium Proton Exchange Activity

Mammalian CHP has been shown to be required for the activity of multiple recombinant sodium-proton exchangers (33, 35, 48, 69). Thus, we hypothesized that intestinal PBO-1

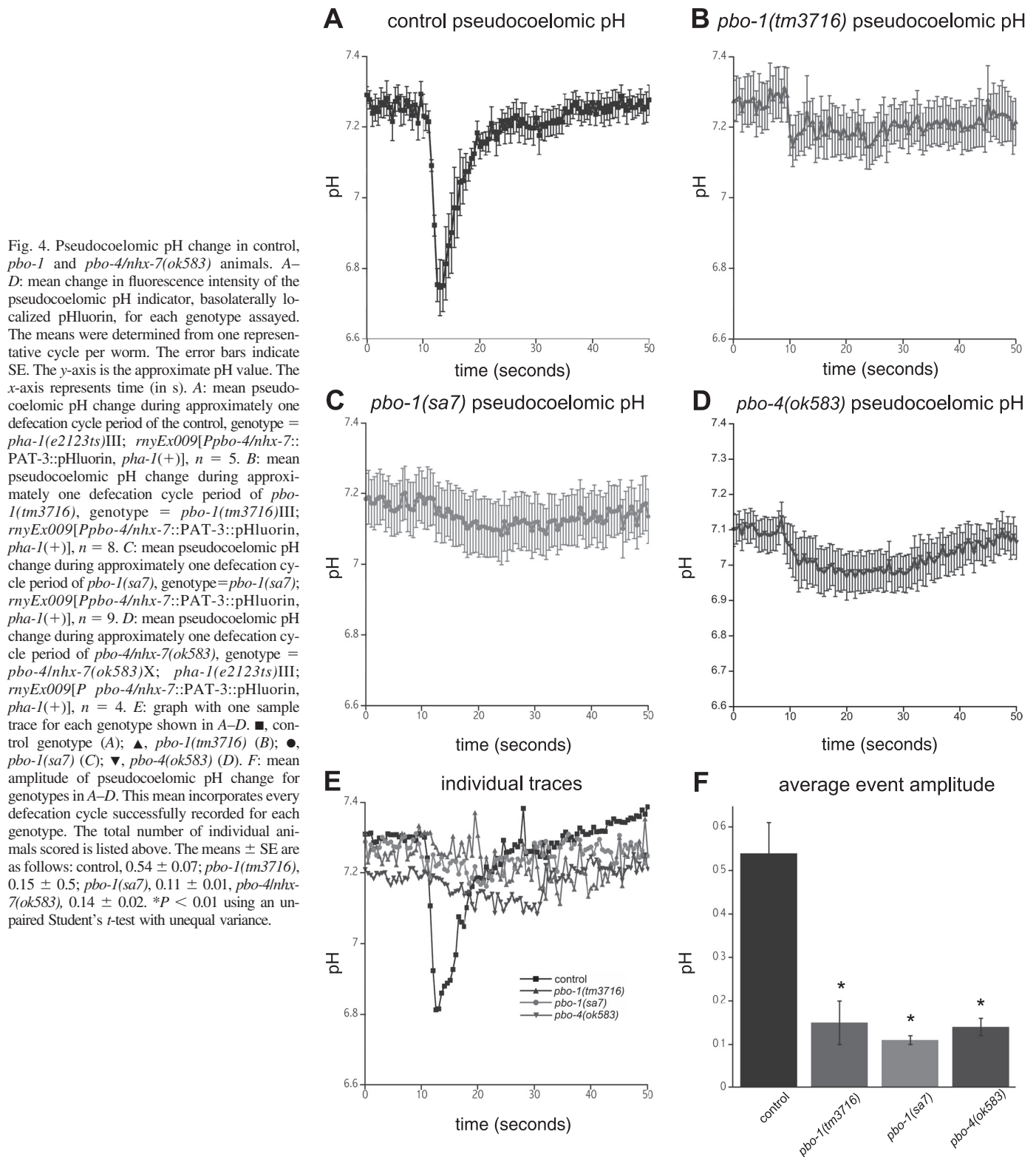


Fig. 4. Pseudocoelomic pH change in control, *pbo-1* and *pbo-4/nhx-7(ok583)* animals. A–D: mean change in fluorescence intensity of the pseudocoelomic pH indicator, basolaterally localized pHluorin, for each genotype assayed. The means were determined from one representative cycle per worm. The error bars indicate SE. The y-axis is the approximate pH value. The x-axis represents time (in s). A: mean pseudocoelomic pH change during approximately one defecation cycle period of the control, genotype = *pha-1(e2123ts)III*; *rnyEx009[Ppbo-4/nhx-7::PAT-3::pHluorin, pha-1(+)]*, *n* = 5. B: mean pseudocoelomic pH change during approximately one defecation cycle period of *pbo-1(tm3716)*, genotype = *pbo-1(tm3716)III*; *rnyEx009[Ppbo-4/nhx-7::PAT-3::pHluorin, pha-1(+)]*, *n* = 8. C: mean pseudocoelomic pH change during approximately one defecation cycle period of *pbo-1(sa7)*, genotype = *pbo-1(sa7)*; *rnyEx009[Ppbo-4/nhx-7::PAT-3::pHluorin, pha-1(+)]*, *n* = 9. D: mean pseudocoelomic pH change during approximately one defecation cycle period of *pbo-4/nhx-7(ok583)*, genotype = *pbo-4/nhx-7(ok583)X*; *pha-1(e2123ts)III*; *rnyEx009[Ppbo-4/nhx-7::PAT-3::pHluorin, pha-1(+)]*, *n* = 4. E: graph with one sample trace for each genotype shown in A–D. ■, control genotype (A); ▲, *pbo-1(tm3716)* (B); ●, *pbo-1(sa7)* (C); ▼, *pbo-4(ok583)* (D). F: mean amplitude of pseudocoelomic pH change for genotypes in A–D. This mean incorporates every defecation cycle successfully recorded for each genotype. The total number of individual animals scored is listed above. The means ± SE are as follows: control, 0.54 ± 0.07 ; *pbo-1(tm3716)*, 0.15 ± 0.5 ; *pbo-1(sa7)*, 0.11 ± 0.01 ; *pbo-4/nhx-7(ok583)*, 0.14 ± 0.02 . **P* < 0.01 using an unpaired Student's *t*-test with unequal variance.

would independently regulate defecation-associated sodium-proton exchange events that occur at the intestine's apical as well as basolateral membrane. Proton movement across the apical membrane, into the cytoplasm, requires the sodium proton exchanger NHX-2 and is thought to prevent the loss of these protons during defecation (51). Since proton motive

forces are important for nutrient uptake, the loss of *nhx-2* expression causes defects in dipeptide absorption by compromising proton-coupled uptake pathways (41). In support of this hypothesis, some of these *pbo-1* and *nhx-2* mutant phenotypes overlap. Specifically, both *nhx-2(RNAi)* and *pbo-1* mutants are small, slow to develop, and produce low broods (41, 51).

Unfortunately, the *nhx-2* posterior body contraction phenotype, extension of the time period of the contraction, could not be assessed in the *pbo-1* mutants through epistasis analysis due to severe developmental defects in the double mutant (K. W. Nehrke, unpublished observations). However, the phenotypic similarity between *pbo-1* and *nhx-2* mutants suggests that PBO-1 may regulate NHX-2. Observing alterations of the

normal luminal and/or cytoplasmic pH cycles in the *pbo-1* mutants would directly support this proposed interaction.

Luminal-to-cytoplasmic proton movement indeed is diminished in *pbo-1* mutants. Luminal pH was monitored shortly following introduction of a pH indicator into the intestinal lumen by acute feeding. In normal animals, luminal pH climbed upward rapidly and then slowly recovered, shifting

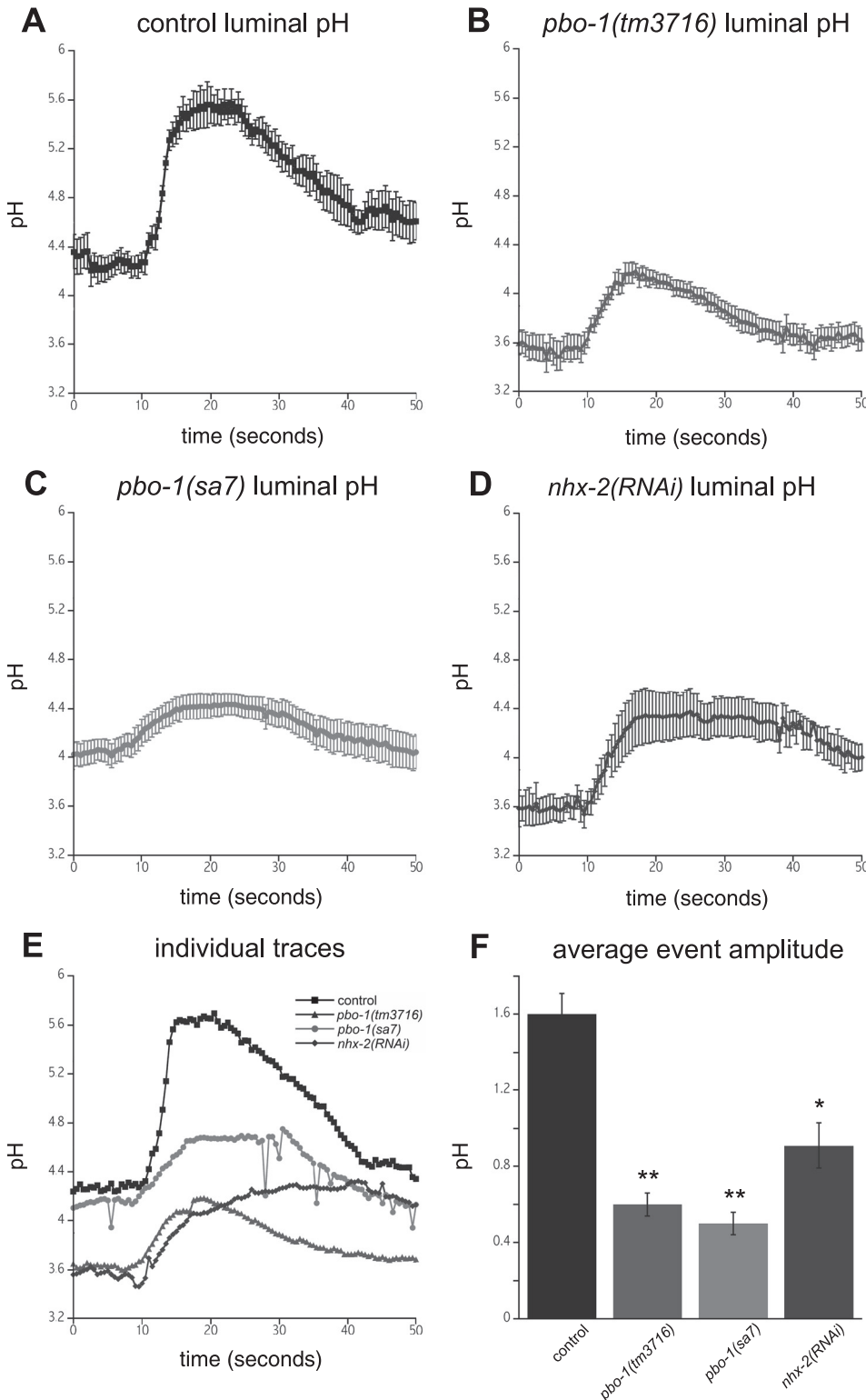
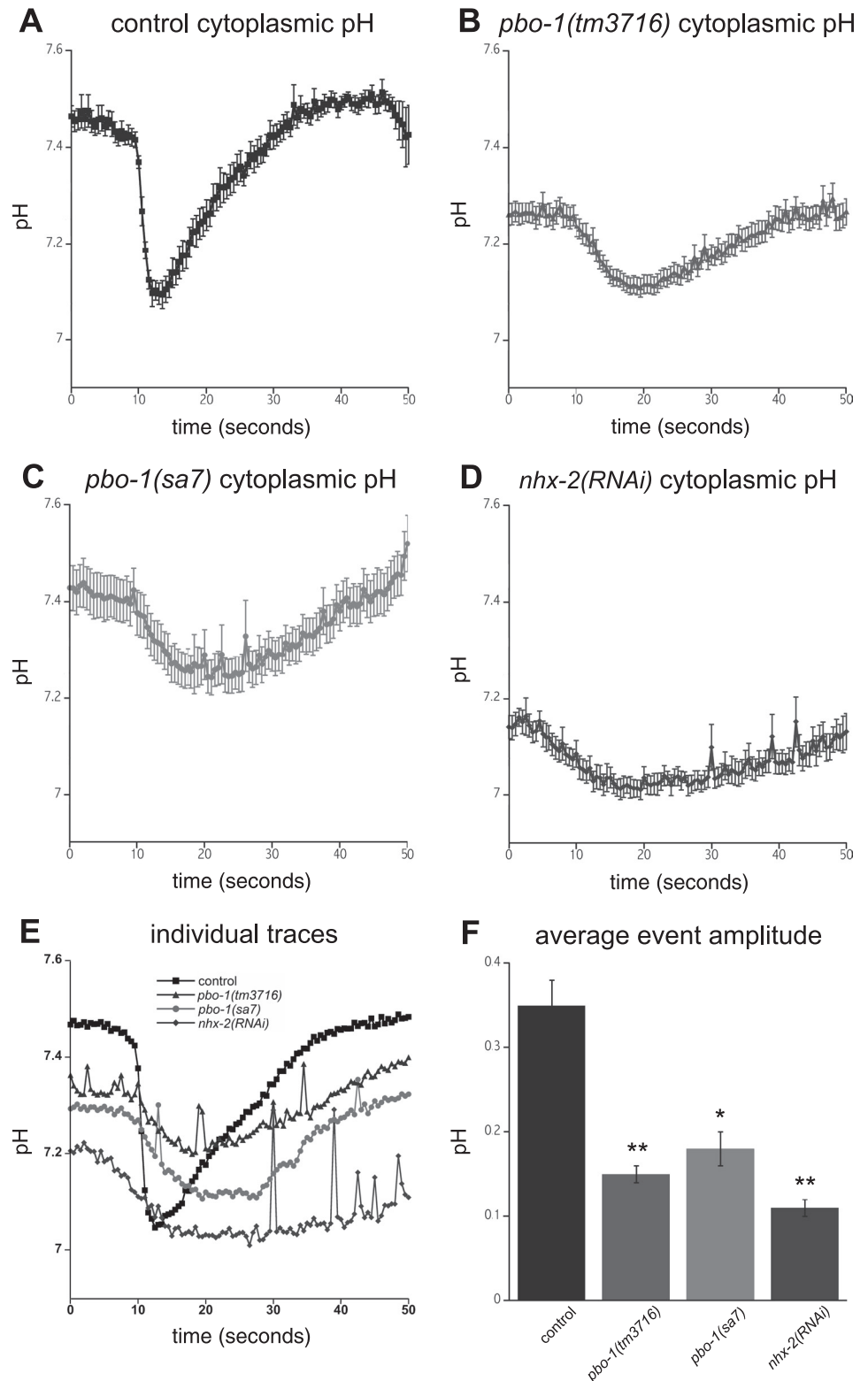


Fig. 5. Luminal pH change in the intestines of control, *pbo-1* and *nhx-2(RNAi)* animals. A–D: mean change in fluorescence intensity of the ingested luminal pH indicator, Oregon Green, for each genotype assayed. The means were determined from one representative cycle per worm. The error bars indicate SE. The y-axis is the approximate pH value. The x-axis represents time (in s). A: mean luminal pH change during approximately one defecation cycle period of the control, wild type/N2, $n = 7$. B: mean luminal pH change during approximately one defecation cycle period of *pbo-1(tm3716)*, $n = 8$. C: mean luminal pH change during approximately one defecation cycle period of *pbo-1(sa7)*, $n = 9$. D: mean luminal pH change during approximately one defecation cycle period of *nhx-2(RNAi)*, $n = 4$. E: graph with one sample trace for each genotype shown in A–D. ■, control genotype (A); ▲, *pbo-1(tm3716)* (B); ●, *pbo-1(sa7)* (C); ◆, *nhx-2(RNAi)* (D). F: mean amplitude of luminal pH change for genotypes in A–D. This mean incorporates every defecation cycle successfully recorded for each genotype. The total number of individual animals scored is listed above. The means ± SE are as follows: control, 1.60 ± 0.11 ; *pbo-1(tm3716)*, 0.60 ± 0.06 ; *pbo-1(sa7)*, 0.50 ± 0.06 , *nhx-2(RNAi)*, 0.91 ± 0.12 . * $P < 0.01$ and ** $P < 0.001$ using an unpaired Student's *t*-test with unequal variance.

over 1.5 pH units in total, every defecation cycle (Fig. 5A; Supplemental Movie 9; control, 1.60 ± 0.11). By contrast, *pbo-1* animals showed sluggish and scant luminal pH increases [Fig. 5, B, C, and E; Supplemental Movie 10; *pbo-1(tm3716)*, 0.60 ± 0.06 ; $P < 0.001$; *pbo-1(sa7)*, 0.50 ± 0.06 ; $P < 0.001$]. The luminal pH alkalization was reduced by approximately

2.5-fold compared with normal (Fig. 5, E and F). A similar luminal pH phenotype has been reported previously in *nhx-2* mutants by Pfeiffer et al. (51) and was confirmed here [Fig. 5D; *nhx-2(RNAi)*, 0.91 ± 0.12 ; $P < 0.01$]. Both the *pbo-1(tm3716)* and the *nhx-2(RNAi)* animals exhibit a lower luminal resting pH in comparison to the control [control, 4.15 ± 0.15 ; *pbo-*

Fig. 6. Cytoplasmic pH change in the intestines of control, *pbo-1*, and *nhx-2(RNAi)* animals. A–D: mean change in fluorescence intensity of the cytoplasmically localized pH indicator, cytoplasmic pHluorin, for each genotype assayed. The means were determined from one representative cycle per worm. The error bars indicate SE. The y-axis is the approximate pH value. The x-axis represents time (in s). A: mean cytoplasmic pH change during approximately one defecation cycle period of the control, genotype = *pha-1(e2123ts)III*; *him-5(e1490)V*; *myEx006[Pnhx-2::pHluorin]*, $n = 8$. B: mean cytoplasmic pH change during approximately one defecation cycle period of *pbo-1(tm3716)*, genotype = *pbo-1(tm3716)III*; *myEx006[Pnhx-2::pHluorin]*, $n = 11$. C: mean cytoplasmic pH change during approximately one defecation cycle period of *pbo-1(sa7)*, genotype = *pbo-1(sa7)III*; *myEx006[Pnhx-2::pHluorin]*, $n = 8$. D: mean cytoplasmic pH change during approximately one defecation cycle period of *nhx-2(RNAi)*, genotype = *pha-1(e2123ts)III*; *him-5(e1490)V*; *myEx006[Pnhx-2::pHluorin]*, feed pRNAi-*nhx-2*, $n = 6$. E: graph with one sample trace for each genotype shown in A–D. ■, control genotype (A); ▲, *pbo-1(tm3716)* (B); ●, *pbo-1(sa7)* (C); ◆, *nhx-2(RNAi)* (D). F: mean amplitude of pH change for genotypes in A–D. This mean incorporates every defecation cycle successfully recorded for each genotype. The total number of individual animals scored is listed above. The means \pm SE are as follows: control, 0.35 ± 0.03 ; *pbo-1(tm3716)*, 0.15 ± 0.01 ; *pbo-1(sa7)*, 0.18 ± 0.02 ; *nhx-2(RNAi)*, 0.11 ± 0.01 . * $P < 0.01$ and ** $P < 0.001$ using an unpaired Student's *t*-test with unequal variance.



l(tm3716), 3.58 ± 0.10 , $P < 0.001$; *pbo-1(sa7)*, 4.10 ± 0.06 ; *nhx-2(RNAi)*, 3.58 ± 0.11 , $P < 0.05$]. The finding that *pbo-1*'s luminal pH dynamics are in close accord with those of *nhx-2(RNAi)* mutants supports our hypothesis that PBO-1 regulates NHX-2 activity.

Further evidence for this interaction comes from examining intracellular pH dynamics. Since proton transfer from the lumen is mirrored by a change in cytoplasmic pH, *pbo-1* mutants should undergo reduced cytoplasmic acidification together with the aforementioned reduction in luminal alkalization. Because of the relative volumes of the cytoplasm and lumen, the normal cytoplasmic pH change is relatively subtle compared with that of the lumen (~4-fold difference in magnitude). In control animals, the intestinal cytoplasm undergoes a quick pH drop followed by slow recovery to resting levels [Fig. 6A; Supplemental Movie 11; 0.35 ± 0.03 ; (51)]. The *pbo-1* animals undergo a more modest alkalization of under 0.2 units [Fig. 6, B, C, E, and F; Supplemental Movie 12; *pbo-1(tm3716)*, 0.15 ± 0.01 , $P < 0.001$; *pbo-1(sa7)*, 0.18 ± 0.02 , $P < 0.01$]. The *pbo-1*'s pH kinetics are also slower than those of wild type, further suggesting that the proton influx pathway is severely compromised. To directly compare the magnitude of *pbo-1*'s and *nhx-2*'s cytoplasmic pH phenotypes, cytoplasmic pH was recorded in several *nhx-2(RNAi)* mutants. The *nhx-2(RNAi)* mutants exhibited weaker and slower cytoplasmic alkalization events that resemble those of *pbo-1* mutants [Fig. 6, D–F; *nhx-2(RNAi)*, 0.11 ± 0.01 , $P < 0.01$; (51)]. Reduced resting cytoplasmic pH is observed in the stronger *pbo-1* allele, *tm3716*, and the *nhx-2(RNAi)* mutants [control, 7.43 ± 0.02 ; *pbo-1(tm3716)*, 7.25 ± 0.02 , $P < 0.001$; *pbo-1(sa7)*, 7.38 ± 0.02 ; *nhx-2(RNAi)*, 7.17 ± 0.02 , $P < 0.001$]. The shared reduction in resting cytoplasmic pH of *pbo-1(tm3716)* and *nhx-2(RNAi)*, but not *pbo-1(sa7)*, animals mirrors the reduction of resting luminal pH noted above. These observations fit nicely with the genetic data suggesting that the *tm3716* allele is the stronger of the *pbo-1* alleles. Both the luminal and the cytoplasmic pH cycles of *pbo-1* and *nhx-2* mutants are altered in analogous manners, suggesting that these proteins act in the same pathway.

Fat Accumulation Decreased in *pbo-1* Mutants

One consequence of reduced NHX-2 activity is ineffective nutrient uptake and associated dietary restriction or, in the absence of activity altogether, starvation. The proton gradient between the intestinal lumen and cytoplasm provides the driving force for the coupled transport of dipeptides and protons into the intestine (41). Consequentially, the lifespan of the *nhx-2(RNAi)* animals is lengthened owing to the effects of caloric restriction on metabolism (41). Since PBO-1 affects the NHX-2-associated proton movements, loss of PBO-1 may also alter the animal's nutritional state. Intestinal fat levels were evaluated using the lipophilic dye Oil Red-O staining to determine whether the *pbo-1* animals were nutritionally compromised (58). In control animals the staining is most prominent in the intestine, in the fat droplets (Fig. 7A). Oil Red-O staining is very limited in the *pbo-1* animals in comparison to control intestines (Fig. 7, A–C). In particular, the intestinal tissue appears to lack any fat staining. Instead, the most prominent Oil Red-O signal is within the gonad, sometimes including the most mature eggs/embryos (Fig. 7, B and C). By contrast,

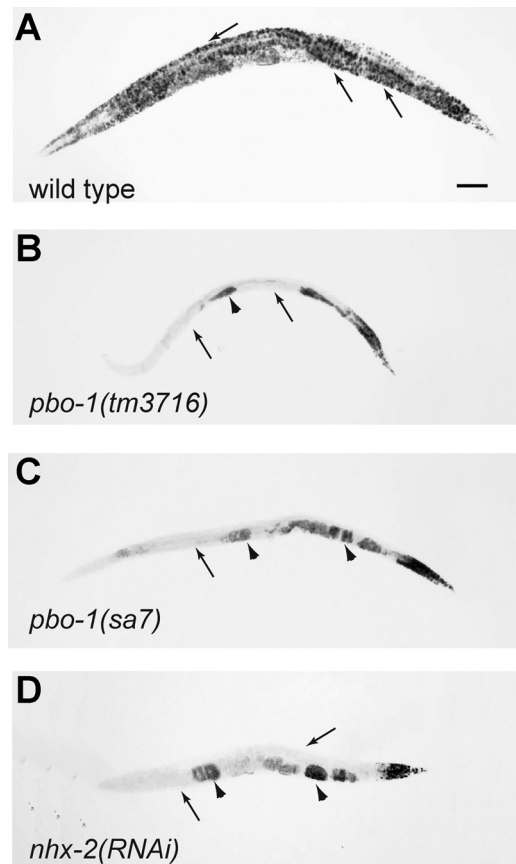


Fig. 7. Fat stores in control, *pbo-1*, and *nhx-2(RNAi)* animals. A–D: fat contents were visualized by Oil Red-O staining. Images were taken at $\times 10$ magnification, and signal appears as dark dots. Arrows point to the intestine and arrowheads point to the gonad. Scale bar equals 50 μm . A: wild-type Oil Red-O staining pattern, genotype = N2. B: *pbo-1(tm3716)* Oil Red-O staining pattern, genotype = *pbo-1(tm3716)*III. C: *pbo-1(sa7)* Oil Red-O staining pattern, genotype = *pbo-1(sa7)*III. D: *nhx-2(RNAi)* Oil Red-O staining pattern, genotype = *pha-1(e2123ts)*III.

control gonads stain in the regions of the gonad with immature gamete precursors (Fig. 7A). The intestinal and gonadal fat staining of *pbo-1* and *nhx-2(RNAi)* correlate well (Fig. 7, B–D). This similarity along with *pbo-1*'s reduced body size and brood size, both hallmarks of caloric restriction, suggest that *pbo-1* function is required for proper nutrient uptake.

DISCUSSION

The *pbo-1* gene codes for a calcineurin homologous protein that contributes to regulated proton exchange in *C. elegans*. PBO-1 is required for the fast release of protons from the intestine that elicits contraction of the overlying body wall muscles during defecation. *pbo-1* mutation results in a profound diminution of both proton flux in the muscle's extracellular milieu and muscle contraction strength. These findings are consistent with PBO-1 regulating proton signaling through the basolateral sodium-proton exchanger, PBO-4/NHX-7 (7, 51).

Interestingly, the posterior body contraction strength in *pbo-1* mutant alleles is weaker than that of a *pbo-4/nhx-7* deletion mutant, yet no significant differences in *pbo-1* and *pbo-4/nhx-7* pseudocoelomic acidifications exist. There are

several possible explanations for this surprising finding. First, the posterior body contractions observed in the absence of PBO-4/NHX-7 may be due to a non-proton-mediated signal from the intestine that is sufficient to induce weak posterior body contraction. This proposed posterior body contraction signal must require PBO-1 to explain the reduction in *pbo-1*'s contraction strength relative to that of *pbo-4/nhx-7*. Second, it is possible that additional basolateral sodium-proton exchangers respond to the intracellular acidification that accompanies defecation, although they may not necessarily function in a strict signaling capacity (51). The loss of *pbo-1* expression would be predicted to suppress their exchange activity as well as that of the main signaling sodium-proton exchanger PBO-4/NHX-7. The contribution of these sodium-proton exchangers to pseudocoelomic acidification is predicted to be subtle, since our imaging did not detect any distinctions between the pseudocoelomic pH flux dynamics in the *pbo-1* and *pbo-4/nhx-7* mutants. One additional intestinal sodium-proton exchanger, *nhx-6*, has been identified, but its functional role has not yet been explored (44).

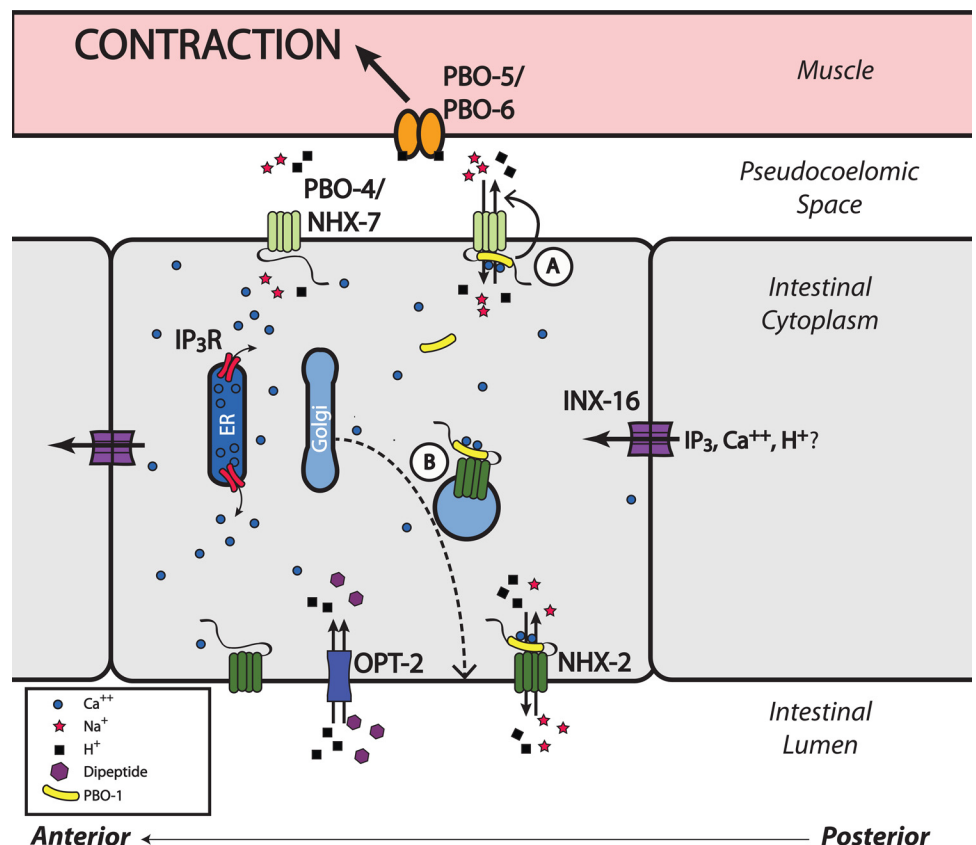
PBO-1's actions are not restricted to the basolateral membrane. *pbo-1* is necessary for the NHX-2-mediated apical sodium-proton exchange events that control intracellular pH, nutrient uptake, and posterior body contraction duration (41). *In vivo* imaging of *pbo-1*'s luminal and cytoplasmic pH indicates a large reduction in proton movement from the acidic lumen into the cytoplasm, a phenotype matching that seen in *nhx-2(RNAi)*-treated worms (51). These changes in the luminal:cytoplasmic proton gradient appear to compromise the proton-coupled nutrient uptake used by the peptide transporter

opt-2/pept-1. As a result, starvation-associated traits, such as reduced fat levels, slow growth, and low fecundity, are exhibited by *pbo-1* mutants. *pbo-1*'s behavioral and physiologic alterations encompass those of two intestinal sodium-proton exchanger mutants, *pbo-4/nhx-7* and *nhx-2*, suggesting that PBO-1 regulates both of their functions (Fig. 8). Although other uncharacterized calcineurin homologous proteins exist in the *C. elegans* genome, it is unlikely that they compensate for PBO-1's regulation of these sodium-proton exchange events given the similarity of *pbo-1*'s phenotypes to those of *pbo-4/nhx-7* and *nhx-2* mutants. Indeed, PBO-1 may be a global regulator of sodium-proton exchange.

The activity of both the apical, NHX-2, and basolateral PBO-4/NHX-7 sodium-proton exchangers occurs in time with the defecation cycle "clock" whose output is intestinal calcium flux. The molecular path linking calcium elevation and activation of sodium-proton exchange is likely to include one or more calcium-responsive proteins. These calcium response factors are expected to bind to the large intercellular COOH-terminal tails of NHX-2 and NHX-7 where virtually all known NHE regulatory proteins act (33). The CHP proteins are calcium-binding proteins that act as essential regulators of sodium-proton exchangers (17, 18, 22, 28, 48, 69). All three vertebrate CHPs bind to multiple NHEs in a conserved region of the COOH-terminal tail, the juxtamembrane region (2, 22, 38, 48, 69). Furthermore, *pbo-4/nhx-7*'s COOH-terminal tail appears to be functionally important; deletion of the entire COOH-terminal tail results in a nonfunctional protein (7).

Several factors suggest that *pbo-1* may function to coordinate cyclic calcium release with sodium-proton exchange

Fig. 8. A model of the signaling pathways governing the initiation of the *C. elegans* posterior body contraction. This schematic diagram shows select membrane transporters and electrolytes in the posterior intestine involved in signaling defecation behavior, highlighting the proposed role of PBO-1 as an NHX accessory protein. Every 45–55 s, a calcium wave is initiated by inositol 1,4,5-trisphosphate receptor (IP₃R) opening and resultant calcium release. The wave propagates, in a posterior-to-anterior fashion, through gap junctions containing the INX-16 protein. PBO-1 contributes to sodium-proton exchange activity at the apical and basolateral membranes. NHX-2 resides in the apical membrane and is physiologically coupled to nutrient uptake via OPT-2/PEPT-1-mediated dipeptide absorption. PBO-1 also contributes to proton efflux at the basolateral membrane via PBO-4/NHX-7, which signals the body wall muscles to contract through activation of the proton receptor PBO-5/PBO-6. This model suggests that PBO-1 may function to acutely regulate the exchange activity of NHX-2 and PBO-4/NHX-7 in response to calcium by conformational changes of the exchanger upon binding (A) and/or by regulating exchanger trafficking or membrane stabilization (B). Accordingly, in the diagram, active sodium-proton exchangers are bound by Ca²⁺-activated PBO-1; by contrast, those exchangers not bound by PBO-1 are inactive. ER, endoplasmic reticulum.



events in the *C. elegans* intestine. First, the ability of adult intestinal *pbo-1* expression to rescue posterior body contraction demonstrates that PBO-1 functions in the adult intestine, the site of the defecation clock. Second, PBO-1 is not required for the initiating calcium spike or wave propagation. Third, sequence homology of vertebrate NHE1 and *C. elegans* NHX-2 and PBO-4/NHX-7 suggests a conserved physical interaction of PBO-1 and these intestinal NHXs (7). Finally, the activation of NHX-2 and NHX-7 is closely tied to calcium flux, and their activity is compromised in *pbo-1* mutants. Our findings are consistent with a model in which calcium elevation induces calcium binding of PBO-1 which results in NHX activation at the plasma membrane, yet other possible sites of interaction are possible (Fig. 8).

Vertebrate studies suggest that CHP may affect multiple processes necessary for sodium-proton exchanger function. The biochemical study of Pang et al. (47) concluded that CHP1 regulated NHE1 by altering its sensitivity to cellular pH (47). This study also suggested a physical association of calcium-bound CHP1 and NHE1 at the plasma membrane under both resting and stimulated conditions. More recent studies have found that CHPs can also function much earlier in the life cycle of exchangers, acting to promote proper maturation and/or localization/stabilization of NHEs at the plasma membrane (28, 35, 48, 69). These findings hint that CHP's effects on sodium-proton exchangers may be multifaceted and/or highly context dependent. Future studies will be necessary to determine exactly what steps in PBO-4/NHX-7's and NHX-2's life cycle are disrupted in the *pbo-1* mutant animals. Using the *C. elegans* systems it will be possible to pinpoint how CHP serves to regulate sodium-proton exchanger activity. Assays exist to survey cellular localization, membrane insertion, and protein levels. Transgenesis allows both normal and genetically engineered forms of both PBO-1 and the NHXs to be tested in vivo.

PBO-1's roles, like mammalian CHPs, may extend beyond regulation of sodium-proton exchange since incongruities between individual sodium-proton exchanger mutants and *pbo-1* mutants were noted (discussed above). The identities of PBO-1's additional binding partners remain to be discovered, but mammalian inquiries provide intriguing candidates. Biochemical studies have identified an array of CHP binding partners including microtubules, glyceraldehyde, kinesin-related motor KIF1B β 2, calcineurin, the DRAK2 protein kinases, and upstream binding factor (3, 23, 25, 34, 40). Studies designed to explore the significance of these biochemical interactions have found that CHPs can regulate calcineurin's phosphatase activity, constitutive vesicle secretion, cytoskeletal organization, proliferation, and cancer metastasis (5, 17, 26, 27, 29, 49, 62).

In conclusion, we have shown that one of the *C. elegans* *chp* orthologs, *pbo-1*, regulates two sodium-proton exchangers. Each of these exchangers responds to a cyclic calcium flux cycle in the intestine that serves to coordinate various important physiologic processes. These findings provide a unique perspective of the physiological consequences of CHP deficiency. Future studies of PBO-1 and other worm CHP orthologs may expand this significant list of functional roles while simultaneously contributing to a more thorough understanding of the physiological relevance of these orthologs within a whole-animal model.

ACKNOWLEDGMENTS

We thank Andrew Burns and Teresa Sherman for technical assistance, Taylor Allen for generously sharing equipment, and Drew Wilburn for help with figure production. The allele *tm3716* was isolated by the National BioResource Project for the Experimental Animal *C. elegans* in Japan. Some strains used in this work were provided by the *Caenorhabditis* Genetics Center, which is funded by the National Institutes of Health National Center for Research Resources. Wormbase was also very useful. Correspondence and requests for reagents should be sent to M. Peters, Maureen.Peters@oberlin.edu.

GRANTS

This work was supported by a National Science Foundation-Research in Undergraduate Institutions (NSF-RUI) 0842830 grant (to M. A. Peters), an NSF IOS0919848 grant (to K. Nehrke), an Institutional Ruth L. Kirschstein National Research Service Award (GM068411, to E. Allman), an NSF/Support of Mentors and Their Students in the Neurosciences award (to M. A. Peters), and Oberlin College funds (to M. A. Peters). The document's contents are solely the responsibility of the authors and do not necessarily represent the official views of the grant awarding institutions or offices.

DISCLOSURES

No conflicts of interest, financial or otherwise, are declared by the author(s).

REFERENCES

1. Allman E, Johnson D, Nehrke K. Loss of the apical V-ATPase α -subunit VHA-6 prevents acidification of the intestinal lumen during a rhythmic behavior in *C. elegans*. *Am J Physiol Cell Physiol* 297: C1071–C1081, 2009.
2. Ammar YB, Takeda S, Hisamitsu T, Mori H, Wakabayashi S. Crystal structure of CHP2 complexed with NHE1-cytosolic region and an implication for pH regulation. *EMBO J* 25: 2315–2325, 2006.
3. Andrade J, Pearce ST, Zhao H, Barroso M. Interactions among p22, glyceraldehyde-3-phosphate dehydrogenase and microtubules. *Biochem J* 384: 327–336, 2004.
4. Andrade J, Zhao H, Titus B, Timm Pearce S, Barroso M. The EF-hand Ca^{2+} -binding protein p22 plays a role in microtubule and endoplasmic reticulum organization and dynamics with distinct Ca^{2+} -binding requirements. *Mol Biol Cell* 15: 481–496, 2004.
5. Barroso MR, Bernd KK, DeWitt ND, Chang A, Mills K, Sztul ES. A novel Ca^{2+} -binding protein, p22, is required for constitutive membrane traffic. *J Biol Chem* 271: 10183–10187, 1996.
6. Baum M, Moe OW, Gentry DL, Alpern RJ. Effect of glucocorticoids on renal cortical NHE-3 and NHE-1 mRNA. *Am J Physiol Renal Physiol* 267: F437–F442, 1994.
7. Beg AA, Ernstrom GG, Nix P, Davis MW, Jorgensen EM. Protons act as a transmitter for muscle contraction in *C. elegans*. *Cell* 132: 149–160, 2008.
8. Bessereau JL, Wright A, Williams DC, Schuske K, Davis MW, Jorgensen EM. Mobilization of a *Drosophila* transposon in the *Caenorhabditis elegans* germ line. *Nature* 413: 70–74, 2001.
9. Brenner S. The genetics of *Caenorhabditis elegans*. *Genetics* 77: 71–94, 1974.
10. Casey JR, Grinstein S, Orlowski J. Sensors and regulators of intracellular pH. *Nat Rev Mol Cell Biol* 11: 50–61, 2010.
11. Choi CH, Patel H, Barber DL. Expression of Aip1 suppresses impaired chemotaxis of *Dictyostelium* cells lacking the Na-H exchanger NHE1. *Mol Biol Cell* 21: 3162–3170, 2010.
12. Croll NA. Behavioural analysis of nematode movement. *Adv Parasitol* 13: 71–122, 1975.
13. Da Silva AC, Reinach FC. Calcium binding induces conformational changes in muscle regulatory proteins. *Trends Biochem Sci* 16: 53–57, 1991.
14. Dal Santo P, Logan MA, Chisholm AD, Jorgensen EM. The inositol trisphosphate receptor regulates a 50-second behavioral rhythm in *C. elegans*. *Cell* 98: 757–767, 1999.
15. Denker SP, Barber DL. Cell migration requires both ion translocation and cytoskeletal anchoring by the Na-H exchanger NHE1. *J Cell Biol* 159: 1087–1096, 2002.
16. Denker SP, Huang DC, Orlowski J, Furthmayr H, Barber DL. Direct binding of the Na-H exchanger NHE1 to ERM proteins regulates the cortical cytoskeleton and cell shape independently of H(+) translocation. *Mol Cell* 6: 1425–1436, 2000.

17. Di Sole F, Babich V, Moe OW. The calcineurin homologous protein-1 increases Na⁽⁺⁾/H⁽⁺⁾-exchanger 3 trafficking via ezrin phosphorylation. *J Am Soc Nephrol* 20: 1776–1786, 2009.
18. Di Sole F, Cerull R, Babich V, Quinones H, Gisler SM, Biber J, Murer H, Burckhardt G, Helmle-Kolb C, Moe OW. Acute regulation of Na/H exchanger NHE3 by adenosine A(1) receptors is mediated by calcineurin homologous protein. *J Biol Chem* 279: 2962–2974, 2004.
19. Donowitz M, Li X. Regulatory binding partners and complexes of NHE3. *Physiol Rev* 87: 825–872, 2007.
20. Espelt MV, Estevez AY, Yin X, Strange K. Oscillatory Ca²⁺ signaling in the isolated *Caenorhabditis elegans* intestine: role of the inositol-1,4,5-trisphosphate receptor and phospholipases C beta and gamma. *J Gen Physiol* 126: 379–392, 2005.
21. Hayashi H, Szaszi K, Grinstein S. Multiple modes of regulation of Na⁺/H⁺ exchangers. *Ann NY Acad Sci* 976: 248–258, 2002.
22. Inoue H, Nakamura Y, Nagita M, Takai T, Masuda M, Nakamura N, Kanazawa H. Calcineurin homologous protein isoform 2 (CHP2), Na⁺/H⁺ exchangers-binding protein, is expressed in intestinal epithelium. *Biol Pharm Bull* 26: 148–155, 2003.
23. Jimenez-Vidal M, Srivastava J, Putney LK, Barber DL. Nuclear-localized calcineurin homologous protein CHP1 interacts with upstream binding factor and inhibits ribosomal RNA synthesis. *J Biol Chem* 285: 36260–36266, 2010.
24. Jin Q, Kong B, Yang X, Cui B, Wei Y, Yang Q. Overexpression of CHP2 enhances tumor cell growth, invasion and metastasis in ovarian cancer. *In Vivo* 21: 593–598, 2007.
25. Kuwahara H, Kamei J, Nakamura N, Matsumoto M, Inoue H, Kanazawa H. The apoptosis-inducing protein kinase DRAK2 is inhibited in a calcium-dependent manner by the calcium-binding protein CHP. *J Biochem* 134: 245–250, 2003.
26. Li GD, Zhang X, Li R, Wang YD, Wang YL, Han KJ, Qian XP, Yang CG, Liu P, Wei Q, Chen WF, Zhang J, Zhang Y. CHP2 activates the calcineurin/nuclear factor of activated T cells signaling pathway and enhances the oncogenic potential of HEK293 cells. *J Biol Chem* 283: 32660–32668, 2008.
27. Li QH, Wang LH, Lin YN, Chang GQ, Li HW, Jin WN, Hu RH, Pang TX. Nuclear accumulation of calcineurin b homologous protein 2 (CHP2) results in enhanced proliferation of tumor cells. *Genes Cells* 16: 416–426, 2011.
28. Lin X, Barber DL. A calcineurin homologous protein inhibits GTPase-stimulated Na-H exchange. *Proc Natl Acad Sci USA* 93: 12631–12636, 1996.
29. Lin X, Sikkink RA, Rusnak F, Barber DL. Inhibition of calcineurin phosphatase activity by a calcineurin B homologous protein. *J Biol Chem* 274: 36125–36131, 1999.
30. Lingueglia E. Acid-sensing ion channels in sensory perception. *J Biol Chem* 282: 17325–17329, 2007.
31. MacMorris M, Broverman S, Greenspoon S, Lea K, Madej C, Blumenthal T, Spieth J. Regulation of vitellogenin gene expression in transgenic *Caenorhabditis elegans*: short sequences required for activation of the *vit-2* promoter. *Mol Cell Biol* 12: 1652–1662, 1992.
32. Maduro MF, Rothman JH. Making worm guts: the gene regulatory network of the *Caenorhabditis elegans* endoderm. *Dev Biol* 246: 68–85, 2002.
33. Malo ME, Fliegel L. Physiological role and regulation of the Na⁺/H⁺ exchanger. *Can J Physiol Pharmacol* 84: 1081–1095, 2006.
34. Matsumoto M, Miyake Y, Nagita M, Inoue H, Shitakubo D, Takemoto K, Ohtsuka C, Murakami H, Nakamura N, Kanazawa H. A serine/threonine kinase which causes apoptosis-like cell death interacts with a calcineurin B-like protein capable of binding Na⁽⁺⁾/H⁽⁺⁾ exchanger. *J Biochem* 130: 217–225, 2001.
35. Matsushita M, Sano Y, Yokoyama S, Takai T, Inoue H, Mitsui K, Todo K, Ohmori H, Kanazawa H. Loss of calcineurin homologous protein-1 in chicken B lymphoma DT40 cells destabilizes Na⁺/H⁺ exchanger isoform-1 protein. *Am J Physiol Cell Physiol* 293: C246–C254, 2007.
36. Meima ME, Mackley JR, Barber DL. Beyond ion translocation: structural functions of the sodium-hydrogen exchanger isoform-1. *Curr Opin Nephrol Hypertens* 16: 365–372, 2007.
37. Miesenbock G, De Angelis DA, Rothman JE. Visualizing secretion and synaptic transmission with pH-sensitive green fluorescent proteins. *Nature* 394: 192–195, 1998.
38. Mishima M, Wakabayashi S, Kojima C. Solution structure of the cytoplasmic region of Na⁺/H⁺ exchanger 1 complexed with essential cofactor calcineurin B homologous protein 1. *J Biol Chem* 282: 2741–2751, 2007.
39. Miyabayashi T, Palfreyman MT, Sluder AE, Slack F, Sengupta P. Expression and function of members of a divergent nuclear receptor family in *Caenorhabditis elegans*. *Dev Biol* 215: 314–331, 1999.
40. Nakamura N, Miyake Y, Matsushita M, Tanaka S, Inoue H, Kanazawa H. KIF1Bbeta2, capable of interacting with CHP, is localized to synaptic vesicles. *J Biochem* 132: 483–491, 2002.
41. Nehrke K. A reduction in intestinal cell pH_i due to loss of the *Caenorhabditis elegans* Na⁺/H⁺ exchanger NHX-2 increases life span. *J Biol Chem* 278: 44657–44666, 2003.
42. Nehrke K. Intracellular pH measurements in vivo using green fluorescent protein variants. *Methods Mol Biol* 351: 223–239, 2006.
43. Nehrke K, Denton J, Mowrey W. Intestinal Ca²⁺ wave dynamics in freely moving *C. elegans* coordinate execution of a rhythmic motor program. *Am J Physiol Cell Physiol* 294: C333–C344, 2008.
44. Nehrke K, Melvin JE. The NHX family of Na⁺-H⁺ exchangers in *Caenorhabditis elegans*. *J Biol Chem* 277: 29036–29044, 2002.
45. Noel J, Pouyssegur J. Hormonal regulation, pharmacology, and membrane sorting of vertebrate Na⁺/H⁺ exchanger isoforms. *Am J Physiol Cell Physiol* 268: C283–C296, 1995.
46. Norman KR, Fazio RT, Mellem JE, Espelt MV, Strange K, Beckerle MC, Maricq AV. The Rho/Rac-family guanine nucleotide exchange factor VAV-1 regulates rhythmic behaviors in *C. elegans*. *Cell* 123: 119–132, 2005.
47. Pang T, Hisamitsu T, Mori H, Shigekawa M, Wakabayashi S. Role of calcineurin B homologous protein in pH regulation by the Na⁺/H⁺ exchanger 1: tightly bound Ca²⁺ ions as important structural elements. *Biochemistry* 43: 3628–3636, 2004.
48. Pang T, Su X, Wakabayashi S, Shigekawa M. Calcineurin homologous protein as an essential cofactor for Na⁺/H⁺ exchangers. *J Biol Chem* 276: 17367–17372, 2001.
49. Pang T, Wakabayashi S, Shigekawa M. Expression of calcineurin B homologous protein 2 protects serum deprivation-induced cell death by serum-independent activation of Na⁺/H⁺ exchanger. *J Biol Chem* 277: 43771–43777, 2002.
50. Peters MA, Teramoto T, White JQ, Iwasaki K, Jorgensen EM. A calcium wave mediated by gap junctions coordinates a rhythmic behavior in *C. elegans*. *Curr Biol* 17: 1601–1608, 2007.
51. Pfeiffer J, Johnson D, Nehrke K. Oscillatory transepithelial H⁽⁺⁾ flux regulates a rhythmic behavior in *C. elegans*. *Curr Biol* 18: 297–302, 2008.
52. Pouyssegur J, Sardet C, Franchi A, L'Allemain G, Paris S. A specific mutation abolishing Na⁺/H⁺ antiport activity in hamster fibroblasts precludes growth at neutral and acidic pH. *Proc Natl Acad Sci USA* 81: 4833–4837, 1984.
53. Putney LK, Barber DL. Na-H exchange-dependent increase in intracellular pH times G2/M entry and transition. *J Biol Chem* 278: 44645–44649, 2003.
54. Rotin D, Steele-Norwood D, Grinstein S, Tannock I. Requirement of the Na⁺/H⁺ exchanger for tumor growth. *Cancer Res* 49: 205–211, 1989.
55. Sankaranarayanan S, De Angelis D, Rothman JE, Ryan TA. The use of pFluorins for optical measurements of presynaptic activity. *Biophys J* 79: 2199–2208, 2000.
56. Simons M, Gault WJ, Gotthardt D, Rohatgi R, Klein TJ, Shao Y, Lee HJ, Wu AL, Fang Y, Satlin LM, Dow JT, Chen J, Zheng J, Boutros M, Mlodzik M. Electrochemical cues regulate assembly of the Frizzled/Dishevelled complex at the plasma membrane during planar epithelial polarization. *Nat Cell Biol* 11: 286–294, 2009.
57. Slepko ER, Rainey JK, Sykes BD, Fliegel L. Structural and functional analysis of the Na⁺/H⁺ exchanger. *Biochem J* 401: 623–633, 2007.
58. Soukas AA, Kane EA, Carr CE, Melo JA, Ruvkun G. Rictor/TORC2 regulates fat metabolism, feeding, growth, and life span in *Caenorhabditis elegans*. *Genes Dev* 23: 496–511, 2009.
59. Teramoto T, Iwasaki K. Intestinal calcium waves coordinate a behavioral motor program in *C. elegans*. *Cell Calcium* 40: 319–327, 2006.
60. Thomas JA, Buchsbaum RN, Zimniak A, Racker E. Intracellular pH measurements in Ehrlich ascites tumor cells utilizing spectroscopic probes generated in situ. *Biochemistry* 18: 2210–2218, 1979.
61. Thomas JH. Genetic analysis of defecation in *Caenorhabditis elegans*. *Genetics* 124: 855–872, 1990.
62. Timm S, Titus B, Bernd K, Barroso M. The EF-hand Ca⁽²⁺⁾-binding protein p22 associates with microtubules in an N-mristoylation-dependent manner. *Mol Biol Cell* 10: 3473–3488, 1999.

63. **Tominaga T, Barber DL.** Na-H exchange acts downstream of RhoA to regulate integrin-induced cell adhesion and spreading. *Mol Biol Cell* 9: 2287–2303, 1998.
64. **Weinman EJ, Steplock D, Donowitz M, Shenolikar S.** NHERF associations with sodium-hydrogen exchanger isoform 3 (NHE3) and ezrin are essential for cAMP-mediated phosphorylation and inhibition of NHE3. *Biochemistry* 39: 6123–6129, 2000.
65. **Wemmie JA, Askwith CC, Lamani E, Cassell MD, Freeman JH Jr, Welsh MJ.** Acid-sensing ion channel 1 is localized in brain regions with high synaptic density and contributes to fear conditioning. *J Neurosci* 23: 5496–5502, 2003.
66. **Wemmie JA, Chen J, Askwith CC, Hruska-Hageman AM, Price MP, Nolan BC, Yoder PG, Lamani E, Hoshi T, Freeman JH Jr, Welsh MJ.** The acid-activated ion channel ASIC contributes to synaptic plasticity, learning, and memory. *Neuron* 34: 463–477, 2002.
67. **Wemmie JA, Coryell MW, Askwith CC, Lamani E, Leonard AS, Sigmund CD, Welsh MJ.** Overexpression of acid-sensing ion channel 1a in transgenic mice increases acquired fear-related behavior. *Proc Natl Acad Sci USA* 101: 3621–3626, 2004.
68. **Wemmie JA, Price MP, Welsh MJ.** Acid-sensing ion channels: advances, questions and therapeutic opportunities. *Trends Neurosci* 29: 578–586, 2006.
69. **Zaun HC, Schrier A, Orlowski J.** Calcineurin B homologous protein 3 promotes the biosynthetic maturation, cell surface stability, and optimal transport of the Na⁺/H⁺ exchanger NHE1 isoform. *J Biol Chem* 283: 12456–12467, 2008.
70. **Ziemann AE, Allen JE, Dahdaleh NS, Drebot II, Coryell MW, Wunsch AM, Lynch CM, Faraci FM, Howard MA 3rd, Welsh MJ, Wemmie JA.** The amygdala is a chemosensor that detects carbon dioxide and acidosis to elicit fear behavior. *Cell* 139: 1012–1021, 2009.

